Journal of Sound and Vibration 329 (2010) 202–220

Contents lists available at ScienceDirect

Journal of Sound and Vibration

journal homepage: www.elsevier.com/locate/jsvi

The horizontal directivity of noise radiated by a rail and implications for the use of microphone arrays

T. Kitagawa [a,1], D.J. Thompson [b,*]

[a] Railway Technical Research Institute, 2-8-38, Hikari-cho, Kokubunji, Tokyo 185-8540, Japan
[b] ISVR, University of Southampton, Highfield, Southampton SO17 1BJ, UK

ARTICLE INFO

Article history:
Received 15 August 2008
Received in revised form
28 July 2009
Accepted 2 September 2009
Handling Editor: C.L. Morfey
Available online 9 October 2009

ABSTRACT

Structural waves propagating along a railway rail form an extended source of sound radiation. Using an equivalent source model the distribution of this sound in a horizontal plane is investigated and shown to consist mainly of sound propagation at a particular angle to the normal. This direction is determined by the ratio of the wavenumbers in the rail and in air. Due to the extended nature of the rail as a source, the spatial distribution of the sound field in the direction along the track does not lend itself to the use of a simple directivity factor. The consequences for the measurement of noise from the rail using a microphone array are then explored. It is shown that a microphone array focussed normal to the rail does not detect most of the sound radiated by the rail. By turning the focus angle, the sound detected becomes a maximum when this angle corresponds to the angle of propagation of the sound radiation. Measurements on a test track using artificial excitation and measurements during the passage of a train confirm these conclusions.

1. Introduction

There are a number of different sources of noise from a moving train. In order to apply appropriate countermeasures it is necessary to understand which noise sources have the greatest contribution to the total in any given situation. Rolling noise, caused by vibrations of the wheels and rails, is important for a wide range of train speeds [1]. At high speeds aerodynamic noise becomes dominant due to its greater speed dependence [2]. Recent studies suggest that aerodynamic noise becomes dominant above about 350 km/h and that rolling noise remains important at 300 or even 320 km/h [3]. Sources of aerodynamic noise include the nose of the leading vehicle, the region around the bogies, inter-coach gaps, pantograph and other roof-mounted equipment [2,4]. Other sources of noise include fans for both traction equipment and air-conditioning, diesel engines and their exhaust systems and electric traction equipment.

Theoretical models have been developed for rolling noise, based on the vibration of the wheels and rails excited by their surface roughness [5]. These models have been validated in terms of the vibration and radiated noise for a range of conventional and novel wheel and track designs [6,7]. Consequently, the relative contributions of the wheel and rail radiation can be considered to be predicted with reasonable reliability. This is especially the case when measurements of wheel and rail vibration are available for use in estimating radiated noise [6–8]. In almost all cases considered, the wheel has been found to be the dominant component for frequencies above about 1.6 kHz, whereas between about 500 and

* Corresponding author. Tel.: +44 23 8059 2510; fax: +44 23 8059 3190.
E-mail addresses: toshiki@rtri.or.jp (T. Kitagawa), djt@isvr.soton.ac.uk (D.J. Thompson).
[1] Tel.: +81 42 573 7353; fax: +81 42 573 7418.

0022-460X/$ - see front matter © 2009 Elsevier Ltd. All rights reserved.
doi:10.1016/j.jsv.2009.09.002

1600 Hz the rail forms the dominant source [6,8]. In terms of overall sound level, the wheel and rail are both important sources, but often, particularly at lower speeds and for track fitted with soft rail pads, the rail has a larger overall contribution than the wheels [6].

An alternative method for identifying sources and determining their relative contributions is to use microphone arrays. These are commonly used to locate acoustic sources on moving vehicles. In particular, trackside microphone arrays are the main means available to identify aerodynamic noise sources on high speed trains [4,9–12]. The same technology has also been used in a number of investigations to quantify the rolling noise contributions from individual wheels of a train [13–18]. However, it has been found that such results often give more prominence to the wheel contribution than to that of the rail, leading to the conclusion that the dominant source is located in the wheel region even for frequencies between 500 and 2000 Hz. In other cases, such as [3], the source appears to be located close to the wheel/rail contact. In contrast to these results, from the theoretical model the rail would be expected to be seen as a source which is extended in length. This therefore appears to conflict with the experimental evidence. It has been shown that the microphone array may not detect most of the sound radiation from the rail, especially if focussed normal to the rail [19]. On the other hand, the wheel is a fairly compact source with a simpler directivity [20] and it is expected that it can be measured successfully using a microphone array.

To investigate this phenomenon further, simulated and measured results are presented of the sound radiation from a rail and the output from a one-dimensional microphone array. A model for the sound radiation from the rail is produced on the basis of an array of simple sources. These are assigned source strengths according to the rail vibration calculated using a beam model. This model allows the distribution of the sound radiation in a horizontal plane to be determined. It is shown from this that the rail forms an extended acoustic source. On the other hand, source identification using a microphone array is based on the (often implicit) assumption that the source region is composed of a distribution of *incoherent* point sources. This is a reasonable assumption for aerodynamic sources, but not for the radiation from an extended source such as the rail. Flexural waves in the rail radiate sound predominantly at an angle to the normal, which is therefore suppressed by an array focussed in a direction normal to the rail. This leads to an underestimation of the contribution of the rail component of noise.

Some initial simulated results from this model were presented in [19], where it was shown that a microphone array directed normal to the track would under-estimate the rail component of noise by 10 dB or more in the frequency region where waves propagate freely along the rail. Consequently, only the radiation from the near-field component of vibration is detected by the array, that from the propagating waves being suppressed by the focussing of the array.

Here, the calculation model for the radiation from the rail is presented and used to simulate in more detail the 'directivity' in a horizontal plane. Strictly, the concept of directivity relies on the source being compact. What is meant in this paper by 'directivity' is the distribution of sound intensity in a two-dimensional plane including the rail axis. For simplicity this plane is considered to be horizontal. The distribution of the sound radiation in the vertical plane normal to the axis of the rail is not considered.

Clearly, sound propagating away from the track is of direct importance to line-side residents. Nevertheless, the 'directivity' in the horizontal plane affects the rise and decay of sound during a train pass-by and is related to the rates of decay of vibration in the track.

These simulations are complemented by two sets of measurements: one on a track excited using a shaker, and the other during the passage of a train. These results confirm the extended nature of the rail as an acoustic source and the inadequacy of source identification based on incoherent sources. The microphone array considered is based on a horizontal one-dimensional array although similar conclusions would be expected where two-dimensional arrays are used for horizontal source location.

2. The directivity of sound radiated by a rail

2.1. Vibration response

The vertical vibration of a railway rail can be represented using a Timoshenko beam for frequencies up to at least 2 kHz [21]. At higher frequencies foot flapping becomes increasingly significant [22]. Lateral vibration is affected by cross-sectional deformation over a wider frequency range; the web-bending wave cuts on at around 1.5 kHz and torsional motion exists at lower frequencies [22]. The point mobility is therefore under-predicted using this model. Nevertheless, the flexural wave remains the dominant source of noise and the beam model can be used to predict the wave motion for this direction also [23,24].

The rail vibration is modelled here as a Timoshenko beam on a continuous two-layer foundation; the sleepers are represented as a layer of mass between damped springs representing the rail pads and the ballast [23,25]. When the rail is excited by a point force, its response can be expressed in terms of waves propagating away from the excitation point. The response of the rail at frequency ω (assuming a time dependence of $e^{i\omega t}$) can be written in the form of a transfer mobility from a force at x=0 to the velocity response at a distance x,

$$Y(x) = (u_1 e^{-ik_1|x|} - iu_2 e^{-\beta_2|x|}) \tag{1}$$

where the wavenumber k_1 corresponds to a propagating wave and β_2 to a near-field wave. These and the corresponding amplitudes u_1 and u_2 are derived in Appendix A. The imaginary part of k_1 corresponds to the decay with distance along the rail,

$$\Delta = -8.686\,\mathrm{Im}(k_1) \tag{2}$$

where Δ is given in dB/m.

Measurements have been taken on a test section of narrow gauge track in Japan laid with type 60 rails and concrete monobloc sleepers in ballast. The nominal sleeper spacing was 0.625 m. Both shaker and hammer excitation were used to determine the point mobility and decay with distance for vertical and lateral vibration. The measurements using shaker excitation were acceptable up to 3 kHz while those using hammer excitation were valid up to at least 5 kHz.

Fig. 1(a) shows the measured and predicted mobility for the vertical direction. For clarity, only the measurements obtained using hammer excitation are shown. The parameters used to model the track are listed in Table 1. Generally good agreement is found, apart from the peak seen in the measurements at 1 kHz. This is due to the pinned–pinned mode of the track, which is not predicted using the continuously supported track model.

Corresponding results for the lateral direction are shown in Fig. 1(b). Here the neglect of torsion and web-bending motion in the model results in an under-prediction of the mobility. Nevertheless, the trends are reproduced in the predictions. The peak at about 500 Hz is again the pinned–pinned resonance.

Fig. 1(c) shows the decay rates for the vertical rail vibration. The measured values were determined from transfer mobility measurements obtained using shaker excitation. To determine the decay rate an integral of the squared vibration over the length of the rail is used [26]. These results also agree quite well with the predictions. The significant fall in the decay rate at around 700 Hz corresponds to the onset of free wave propagation in the rail. At lower frequencies the effects

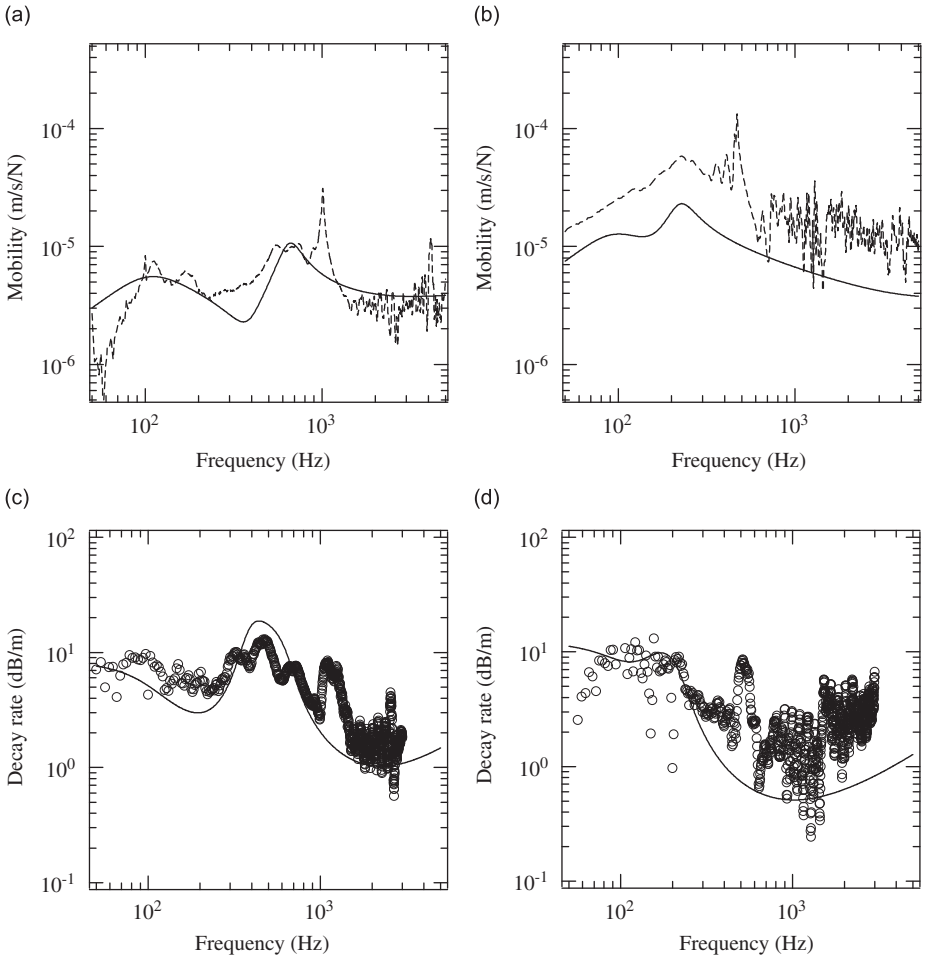

Fig. 1. (a, b) Point mobility for vertical (left) and lateral (right) rail vibrations. ---, measured results between sleepers from hammer excitation; —, predicted results, continuously supported track model. (c, d) Decay rate of vertical (left) and lateral (right) rail vibrations. —, Predicted for propagating wave; ○, measured values.

Table 1
Values of parameters used for the track.

	Vertical	Lateral
Rail bending stiffness (Nm^2)	6.49×10^6	1.08×10^6
Rail shear coefficient	0.4	0.4
Rail loss factor	0.02	0.02
Mass per length (kg/m)	60	
Cross receptance level (dB)	−12	
Pad stiffness (N/m)	4.1×10^8	4.5×10^7
Pad loss factor	0.3	0.3
Sleeper mass (1/2 sleeper) (kg)	80	
Distance between sleepers (m)	0.625 (0.6–0.65)	
Ballast stiffness (N/m)	2.3×10^7	2.0×10^7
Ballast loss factor	2.0	2.0

of sleeper bending modes, neglected in the model, can be seen in oscillations of the measured decay rate in the region 300–800 Hz. The measurements show a peak in the decay rate just above 1 kHz, which is not reflected in the predictions. Again, this is caused by the effect of the periodic support.

The decay rate for the lateral excitation is shown in Fig. 1(d). The measured results are somewhat higher than the model predicts, but follow the same trends.

2.2. Equivalent source model

As shown in [27], below 1 kHz the radiation ratio of a rail resembles that of a line dipole, while above 1 kHz it is close to unity. The sound power and the directivity in a vertical plane (normal to the rail axis) can be predicted reasonably well using a two-dimensional boundary element model [27]. The purpose of the present work is to study the distribution of the sound radiation from a rail in a two-dimensional plane including the rail axis. For simplicity this plane is considered to be horizontal.

To calculate the sound radiation due to the vibration of the rail, an equivalent source model is used [27]. The rail is replaced by a line array of N monopoles located with equal spacing D along its axis. The source separation D must be less than a quarter of the acoustic wavelength at the frequency of interest, as well as less than a quarter of the structural wavelength. A different source spacing is chosen for each frequency according to this criterion. Although dipole sources would give a more realistic directivity in the vertical plane, the results presented here are found not to differ greatly whether monopoles or dipoles are used. Monopoles are therefore used for simplicity.

The volume velocity amplitude of source n is denoted by Q_n and its location by $\mathbf{r}_n$. The distance from the origin along the axis of the rail (the x axis) is denoted by x_n. A series of receiver locations are considered, defined by vectors $\mathbf{r}_m$. The distance between source n and receiver location m is denoted by $R_{mn}=|\mathbf{r}_m-\mathbf{r}_n|$.

For each frequency, ω, the sources are assumed to be mutually coherent, so that their relative phase is taken into account. Then the sound pressure amplitude at receiver location m is given by

$$p(\mathbf{r}_m) = \mathrm{i}\rho_0 c_0 k \sum_{n=1}^{N} \frac{Q_n}{4\pi R_{mn}} \mathrm{e}^{-\mathrm{i}kR_{mn}} \tag{3}$$

where ρ_0 is the density of air, c_0 is the speed of sound in air and $k=\omega/c_0$ is the acoustic wavenumber. Similarly, by differentiating the above, the particle velocity can be written as

$$\mathbf{u}(\mathbf{r}_m) = \sum_{n=1}^{N} (1 + \mathrm{i}kR_{mn}) \frac{Q_n(\mathbf{r}_m - \mathbf{r}_n)}{4\pi R_{mn}^3} \mathrm{e}^{-\mathrm{i}kR_{mn}} \tag{4}$$

The complex volume velocity amplitudes Q_n are chosen to correspond to the vibration velocity of the rail, calculated according to Eq. (1),

$$Q_n = Q_0 Y(x_n) \tag{5}$$

where Q_0 is a constant 'calibration factor' which depends on the separation between the sources and the size of the rail cross-section. This model neglects the effects of the rail cross-section geometry, although these can in principle be included into Q_0. However, as the interest is to determine the directivity in the direction along the track (x direction), not the radiated power or the directivity within the y–z plane, the present model is sufficient and it is not necessary to determine Q_0.

The model could be extended to represent the rail using an array of dipoles by simply taking pairs of sources at each location x_n, separated by a small distance in the transverse direction.

2.3. Results for continuously supported rail

The calculations presented here are based on the vertical track vibration obtained using the model of Section 2.1. The parameters are listed in Table 1. The rail is excited by a point force at x=0; vibration is transmitted symmetrically to either side. The complex vibration amplitude is determined at many points along the rail using Eq. (1). This vibration is used to define the complex source strengths Q_n of a set of point sources located along the axis of the rail, as described above. The sound field due to these point sources is then calculated in terms of the pressure and particle velocity at a number of receiver positions. The time-averaged sound intensity can also be determined from Eqs. (3, 4),

$$\mathbf{I} = \tfrac{1}{2}\mathrm{Re}(p\mathbf{u}^*) \tag{6}$$

Fig. 2 shows the relative sound pressure level induced by vertical rail vibration at four example frequencies. This is plotted against distance along the track for various distances from the rail. The magnitude of the rail vibration is also shown on the same graph. The sound pressure and velocity levels have been plotted to arbitrary reference values to allow them to be plotted together. The highest sound pressure level curve (at least at x=0) corresponds to a distance of 0.5 m from the rail, the subsequent ones to 1, 2 and 4 m.

At 125 Hz the track vibration consists only of strongly decaying waves with a decay rate of around 4 dB/m, as seen in Fig. 1(c). The source is therefore localised to a region close to the forcing point. At 400 Hz the decay rate reaches a peak of almost 20 dB/m and the sound is again radiated only from the vicinity of the forcing point.

At higher frequencies, propagating waves are transmitted along the rail over a significant length of the track. At 800 Hz the decay rate is about 3 dB/m, and at 1600 Hz it is 1 dB/m. The radiation from the rail therefore extends over a considerable length, as seen in Fig. 2(c,d). Particularly for 1600 Hz, it can be seen that the radiated level is relatively low for small values of x and reaches a peak at some distance away from the forcing point. This distance increases as the receiver is moved further away from the track; at 2 m from the track it is x=1.0 m while at 4 m away it is at x=1.9 m. This effect is due to the propagating wave in the rail, which radiates sound at an angle to the normal.

To illustrate this further, Fig. 3 shows the vector of the time-averaged sound intensity calculated at various positions relative to the rail. The intensity vectors are shown with their lengths proportional to the intensity level in dB, with a dynamic range of 25 dB.

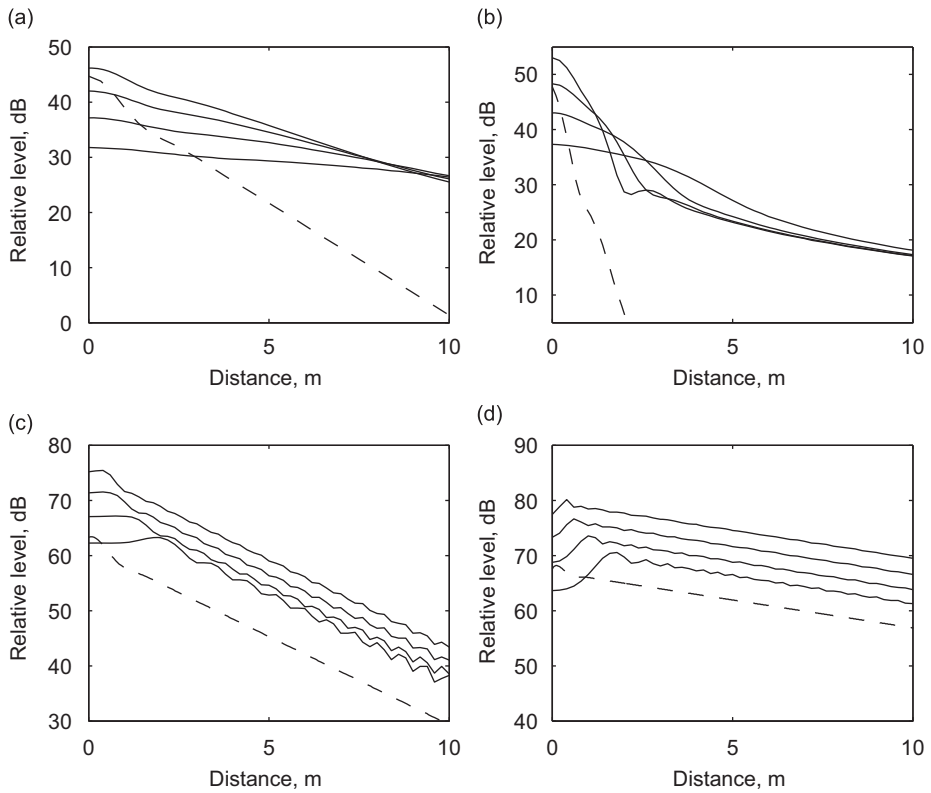

Fig. 2. Sound radiation from a rail versus distance along the track from the forcing position: —, relative sound pressure level at various lateral distances (0.5, 1, 2, and 4 m) from the rail; – – –, relative source strength obtained from vertical rail vibration. Relative levels shown to arbitrary reference. (a) 125 Hz, (b) 400 Hz, (c) 800 Hz, and (d) 1600 Hz.

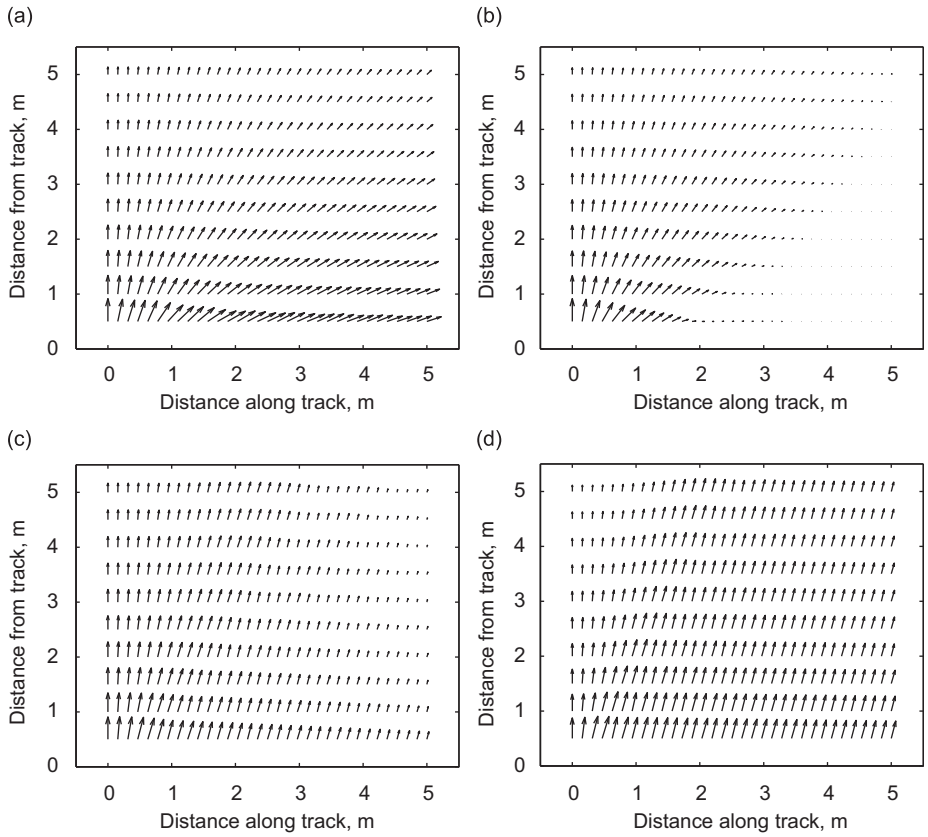

Fig. 3. Sound intensity predicted due to rail vibration at various frequencies. Intensity vectors are shown scaled in decibels with a range of 25 dB. (a) 125 Hz, (b) 400 Hz, (c) 800 Hz, and (d) 1600 Hz.

At 125 Hz the sound radiation can be seen to be approximately omnidirectional relative to the forcing point (0, 0). At 400 Hz the sound is again radiated only from the vicinity of the forcing point. Due to the interaction between the two near-field waves in the rail at this frequency, the radiation is contained within a region around $\pm 45^\circ$ relative to the plane of the forcing point.

At the higher frequencies the radiation from the rail extends over a considerable length, as already seen in Fig. 2. Of particular note is the direction of the intensity vectors. Apart from the region close to the forcing point at x=0, the direction of the intensity vector is close to that determined by the wavenumbers in the rail, k_1, and in air, k_{air}. For example, at 1600 Hz, Re(k_1)=6.55 rad/m and k_{air}=29.3 rad/m, giving an angle to the normal of $\sin^{-1}(\mathrm{Re}(k_1)/k_{air})=12.9^\circ$. This agrees closely with the angle observed at most of the points shown.

It is clear from these results that, due to the extended nature of the rail as a source, the spatial distribution of the sound field in the direction along the track does not lend itself to the use of a simple directivity factor, for which the intensity would have to be orientated radially from a single source location, with an angular distribution that does not depend on radial distance.

2.4. Results for periodically supported rail

The above results have been based on the vibration predicted using a continuously supported track model. As seen in Fig. 1, the periodic support has noticeable effects on the vibration in the vicinity of the pinned–pinned mode, which occurs for vertical vibration at 1 kHz and for lateral vibration at 500 Hz. Therefore the above analysis has been repeated using a model for the rail vibration based on a discretely supported Timoshenko beam [28].

Example results are shown in Fig. 4. These only differ significantly from the results for a continuously supported beam model in the region around 1 kHz. Thus the results for 800 and 1600 Hz in Fig. 4(a,d) closely resemble those in Fig. 3(c,d) and the continuously supported beam model appears adequate at these frequencies. However, the results for 1000 and 1250 Hz reveal strong periodic effects within the radiated field. At 1000 Hz, the direction of the intensity vector varies from 0° up to 54° and the magnitude also varies considerably. At 1250 Hz the variations are smaller but the radiation still differs considerably from that for a continuously supported beam.

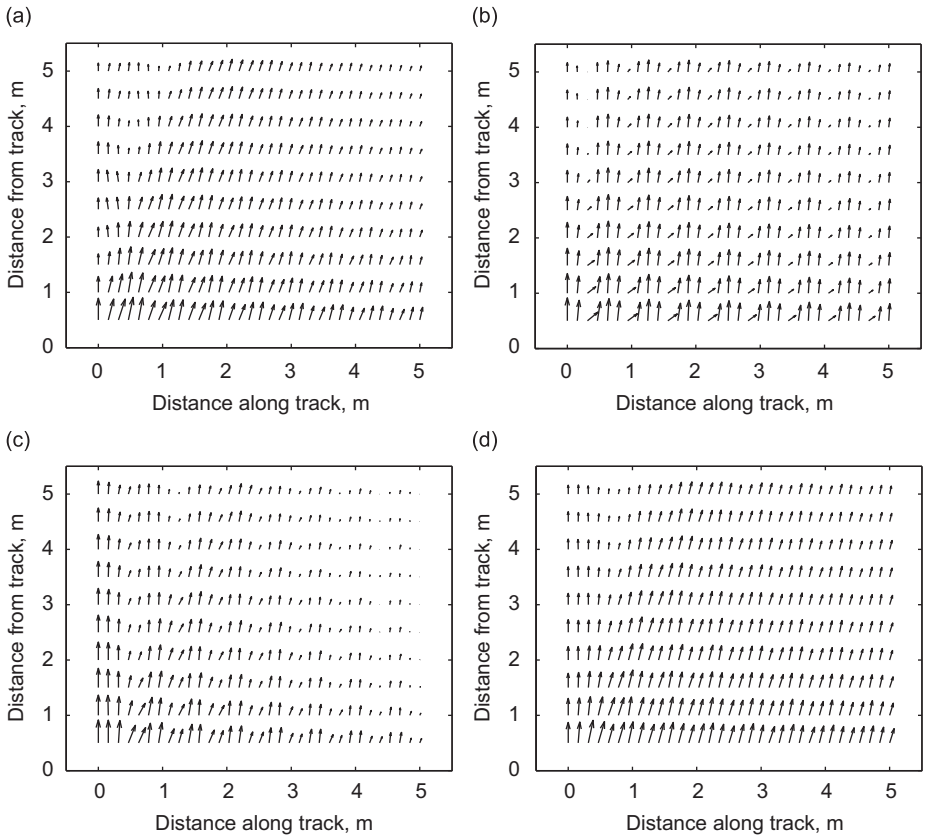

Fig. 4. Sound intensity predicted due to rail vibration at various frequencies, based on discretely supported rail model. Intensity vectors are shown scaled in decibels with a range of 25 dB. (a) 800 Hz, (b) 1000 Hz, (c) 1250 Hz, and (d) 1600 Hz.

3. Acoustic measurements for track excited by shaker

3.1. Description of the acoustic measurements

Acoustic measurements were carried out for the same track as described above, located in the open air, using a one-dimensional horizontal microphone array. The rail was excited first in the vertical direction and then in the horizontal direction by using a shaker. The shaker was driven by a pure tone from a signal generator at each of eight one-third octave band centre frequencies between 500 and 2500 Hz. Fig. 5 shows the measurement locations used for the vertical and horizontal excitation. In order to minimise acoustic radiation from the shaker itself, this was enclosed in a steel box, the interior of which was covered with sound absorbing material. In addition, the microphone array was located quite close to the rail to minimise the effects of noise from the shaker.

The axis of the microphone array was orientated parallel to the rail and the focus angle was varied by introducing different time delays between the measured pressure signals. Measurements were carried out with the centre of the array located at several receiver positions along the rail, between 1.5 and 5 m from the forcing point.

The microphone array used is a simple one-dimensional array composed of 13 microphones. For any given frequency only nine of these are used. For frequencies up to 1250 Hz, the microphones used have an equal spacing of 0.136 m, giving an array length of 1.088 m. For frequencies from 1600 to 2500 Hz, the microphones used have a spacing of 0.068 m giving an array length of 0.544 m. At both 1250 and 2500 Hz, therefore, the microphone spacing is equal to half the acoustic wavelength and may be described as optimal. The sound pressure signals from each microphone were recorded for subsequent processing. This processing consisted of a delay-and-sum process using Dolph-Tschebyscheff weighting factors [29]. The processing was designed to direct the focus of the array at a series of angles to the normal by using different delays. The array processing was based on the assumption of an incoming plane wave (the implications of this are discussed below).

This array is simpler than those often used in practical applications with a smaller number of microphones and therefore has a more limited spatial resolution. Nevertheless it is useful for making comparisons between measurements and predictions, as well as for demonstrating the principles under investigation here.

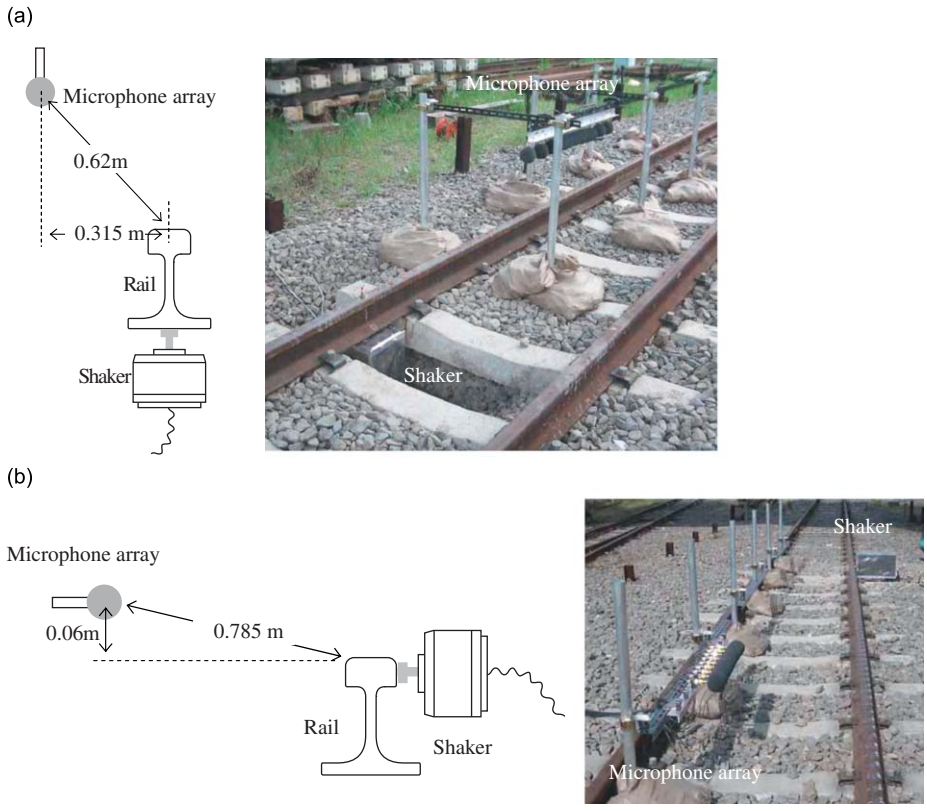

Fig. 5. Setup for the sound measurements of the vertical (a) and lateral (b) shaker excitation.

Similar array processing was also applied to the predicted sound pressures obtained using the model of Section 2. For this simulated data the complex pressure amplitudes p_m were predicted at each microphone position and the delay-and-sum procedure was implemented in the frequency domain.

3.2. Simulations of array performance

Before considering the results of these acoustic measurements for the track, the microphone array is briefly discussed. Simulations are presented here for a linear array with 9 microphones, with a spacing of 0.136 m. The array processing uses Dolph-Tschebyscheff weighting factors [29] and can be based either on an assumption of an incoming plane wave at some angle of incidence, or on an incoming spherical wave originating at some focus point.

Fig. 6 shows results simulated for the array at two frequencies, 800 and 1250 Hz, using processing on the basis of plane waves. Fig. 7 shows equivalent results for spherical wave processing in which the source is assumed to lie somewhere on a line at 3 m from the array axis. The 'relative level' means the difference in dB between the output of the microphone array and the average of the squared pressure at the 9 microphones used for this frequency. In all these simulations, the actual source being detected consists of an incoming plane wave with various angles of incidence. Clearly, the array processing based on an assumption of plane waves (Fig. 6) gives a better resolution of this angle than the spherical wave processing (Fig. 7) for this source.

If the microphone spacing is reduced to 0.068 m, the results for 2500 Hz are identical to those for 1250 Hz in Fig. 6, as the ratio of microphone spacing to wavelength is identical.

In addition, equivalent results have been simulated for a point monopole source. In this case (not shown), provided that the distance to the source is known, the spherical wave processing gives results that are almost identical to those in Fig. 6, while the plane wave processing gives results that are almost identical to those in Fig. 7. Thus the best resolution is obtained when the array processing is chosen to match the form of the incoming wave.

In Fig. 6 the width of the main lobe increases only slightly for 15° and 30° compared with 0° but it is much wider for 45° (and above). The width of the main lobe reduces as frequency increases. The side lobes are about 20 dB lower than the main lobe for this arrangement of microphones with the Dolph-Tschebyscheff weighting factors.

Fig. 8 shows results for a longer array with 13 microphones, again at a spacing of 0.136 m. These results are for an incoming plane wave at 1250 Hz processed using the plane wave assumption. Compared with Fig. 6(b) the main lobe has

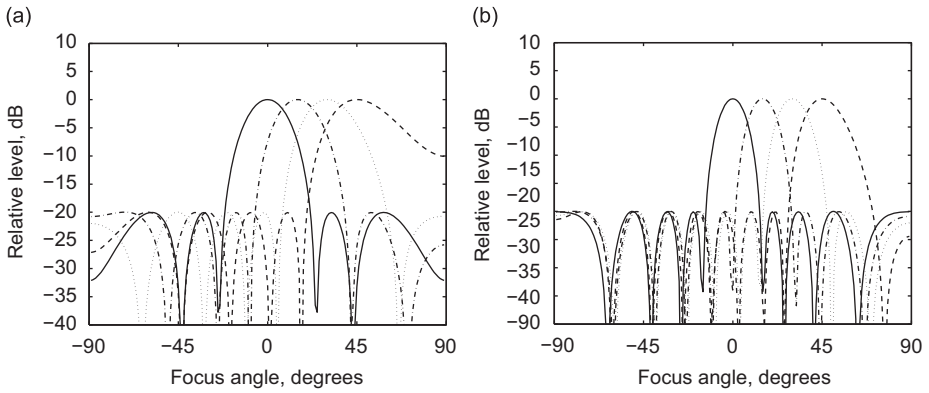

Fig. 6. Output from array of 9 microphones normalised by average squared pressure on microphones. Incident plane wave with spherical wave processing for assumed source location at 3 m perpendicular distance. (a) 800 Hz; (b) 1250 Hz. Incident angle: —, 0°; – · – ·, 15°; · · · · · ·, 30°; – – –, 45°.

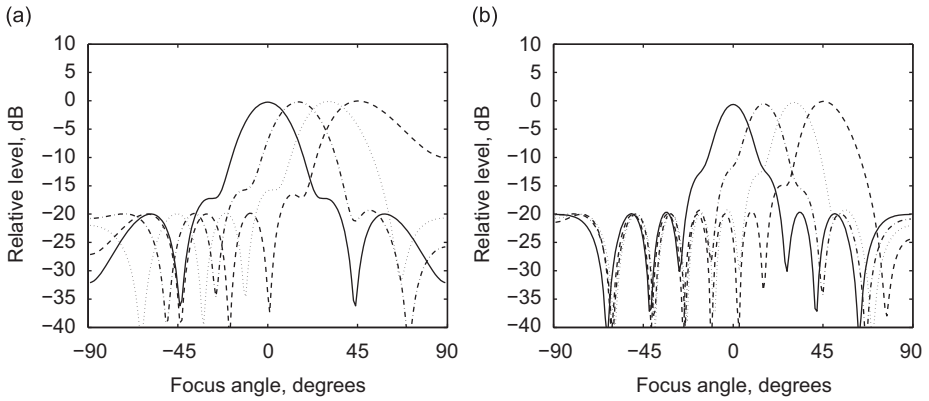

Fig. 7. Output from array of 9 microphones normalised by average squared pressure on microphones. Incident plane wave with spherical wave processing for assumed source location at 3 m perpendicular distance. (a) 800 Hz, and (b) 1250 Hz. Incident angle: —, 0°; — · –, 15°; · · · · · ·, 30°; – – –, 45°.

become narrower and the side lobes have been reduced in level. This indicates the limitations of the present array in terms of beam width and side lobe suppression. However, despite its somewhat coarse resolution it is sufficient for the purposes of this paper.

3.3. Radiation behaviour of a rail

The investigation of the measured radiation behaviour of the rail is carried out for different focus angles of the microphone array. These vary between -60° and $+60^\circ$ to the normal, although it has been noted in Section 3.2 that, for angles above 30°, the beam width is greater and the resolution less good. Measured results are compared with predictions based on the continuously supported track model combined with the equivalent source model, as described in Section 2.

Fig. 9(a) shows the radiation characteristics of the rail obtained at 500 Hz for different focus angles of the microphone array. The array is centred at a distance of 3.12 m from the forcing point. Also shown are the outputs obtained with the microphone array if the predicted source distribution is used and the sources are assumed to be a line array of coherent monopoles. For comparison, the results are shown that would be obtained if these sources were incoherent.

At this frequency, the rail vibration is localised in a region around the forcing point due to high decay rate, measured to be about 10 dB/m. This effectively forms a point source. Consequently the microphone array gives a maximum output when it is directed towards the excitation point, which is at an angle of -78° from the centre of the array for this location. This can be seen from the direction of the intensity vectors in Fig. 3(b).

In this case the overall trends in the measured results are fairly well predicted by both the coherent and incoherent sources. The maximum gain can be seen to occur at the minimum angle considered, -60°. Fig. 9(b) shows the focus angle that gives the maximum gain determined from this process, as a function of the distance of the array from the forcing point, which is close to -60° for distances above 2 m for both predictions and measurements.

Fig. 10 shows results for 800 Hz. At this frequency free wave propagation occurs in the rail with a decay rate of 3 dB/m and the rail effectively represents an extended line source. The rail therefore radiates sound at an angle to the normal. By

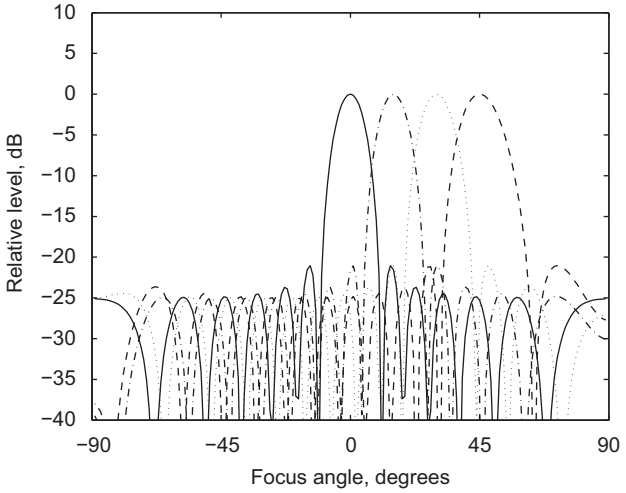

Fig. 8. Output from array of 13 microphones normalised by average squared pressure on microphones. Incident plane wave with plane wave processing at 1250 Hz. Incident angle: —, 0°; – · – · , 15°; · · · · · · , 30°; – – –, 45°.

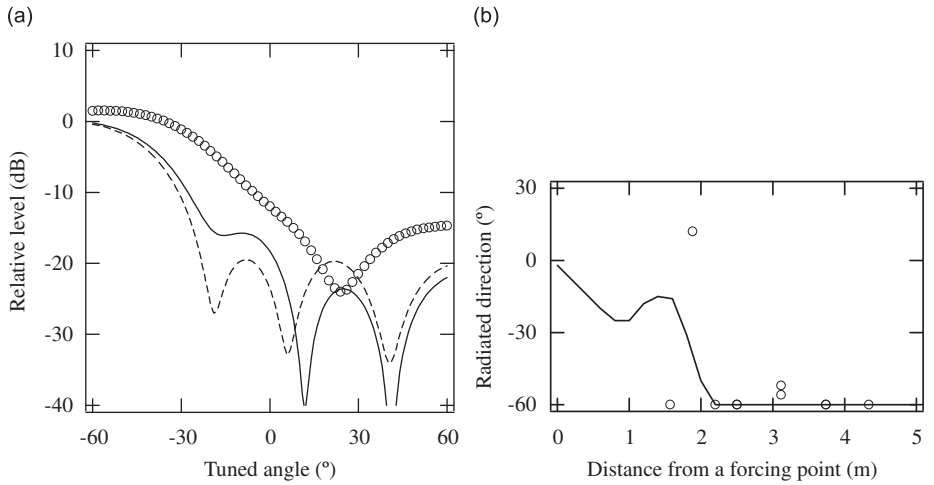

Fig. 9. Measured and predicted results for vertical shaker excitation at 500 Hz. (a) Radiation pattern measured at a distance of 3.12 m from the forcing point. ○, Measured results; —, predictions for coherent sources; - - -, predictions for incoherent sources. (b) Direction of main lobe in the radiation pattern. ○, Measured results; —, predictions for coherent sources.

steering the array axis, a clear peak can be seen for a focus angle of about 15° in the measured results. Conventional interpretation of microphone array measurements might suggest that a strong source is located at a point at 15° from the centre of the array. However, the source is actually extended along the rail, as seen from the rail vibration measurements. This angle of 15° corresponds to the direction of the intensity vectors seen in Fig. 3(c) and is related to typical supersonic structural radiation, whose radiation direction is determined by the ratio of the structural and acoustic wavelengths. The direction of the peak is found to be largely independent of the location of the microphone array along the rail between 1.5 and 3 m. These measured results show good agreement with the prediction based on coherent sources for this main lobe. This confirms that it is appropriate to represent the vibrating rail as a line array of coherent sources. If the rail is modelled instead using incoherent sources the results give poor agreement with the measurements.

The agreement for other tuned angles is less good, possibly due to the proximity of the array to the rail. Nevertheless, these results are mostly around 10 dB lower than those for the main lobe. Spherical wave processing (not shown) gives a much less clear picture in this case.

Fig. 11 shows results for 1000 Hz. Here, results at a position x=3.74 m are shown; those at 3.12 m show a much less clear directional behaviour [29]. At this frequency, strong undulations related to the pinned–pinned resonance are found in the amplitudes of the rail vibration measured along the rail, which are not present in the predictions based on a continuously supported rail. The predicted results, therefore, show less good agreement with the measurements. This is due to the fact

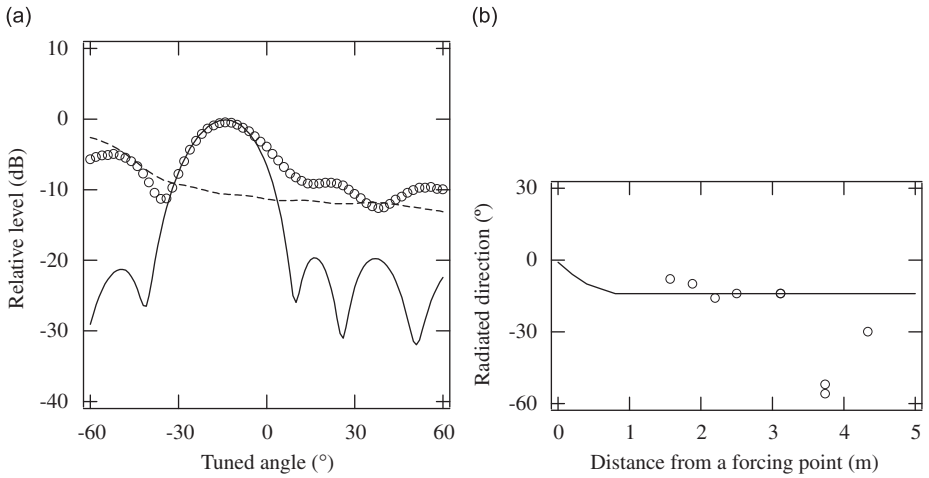

Fig. 10. Measured and predicted results for vertical shaker excitation at 800 Hz. (a) Radiation pattern measured at a distance of 3.12 m from the forcing point. ○, Measured results; —, predictions for coherent sources; - - -, predictions for incoherent sources. (b) Direction of main lobe in the radiation pattern. ○, Measured results; —, predictions for coherent sources.

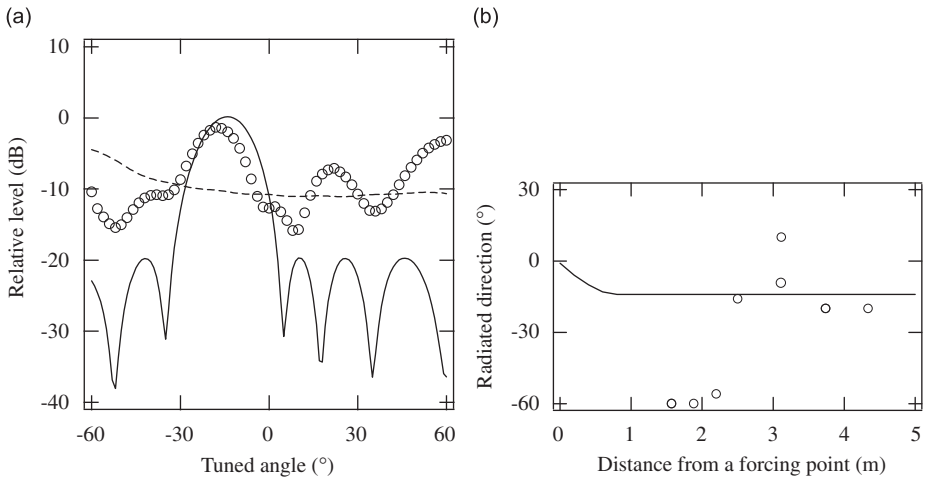

Fig. 11. Measured and predicted results for vertical shaker excitation at 1000 Hz. (a) Radiation pattern measured at a distance of 3.12 m from the forcing point. ○, Measured results; —, predictions for coherent sources; - - -, predictions for incoherent sources. (b) Direction of main lobe in the radiation pattern. ○, Measured results; —, predictions for coherent sources.

that the vibratory behaviour induced by the pinned–pinned resonance has a significant influence on the radiation characteristics of the rail, as seen in Fig. 4(b). The microphone array used at this frequency has a length of over 1 m so there will be considerable variation in the direction and magnitude of the incoming sound intensity along the array. As well as the main lobe at 15° seen in the predictions, the measured results indicate a strong lobe at −15° corresponding to waves in the negative-going direction.

Figs. 12 and 13 show results for 1600 and 2000 Hz. At these frequencies free wave propagation again occurs in the rail. A clear peak can be seen at about 13–15° in the measured results. This corresponds to the direction seen in Fig. 3(d), determined by the ratio of the structural and acoustic wavelengths. In Figs. 12(b) and 13(b) the direction of the peak is found to be largely independent of the location of the microphone array along the rail. These measured results show very good agreement with the prediction based on coherent sources, at least at the main lobe.

Similar trends to these are found in the results for lateral excitation for most frequencies. Examples are shown in Figs. 14 and 15. The direction of the main lobe is between 20° and 30° as the wavenumber of lateral bending waves is smaller than that for vertical bending. Good agreement is seen between the measurements and predictions based on coherent sources at the main lobe.

Fig. 16 summarises the results for all frequencies by showing the focus angle of the main lobe for both vertical and horizontal directions. For each frequency a range of measured values is shown, obtained for different locations of the microphone array. The results can be seen to be predicted reasonably well in the frequency range where free propagating wave motion occurs in both vertical and horizontal directions (results are therefore not shown for 500 Hz for the vertical

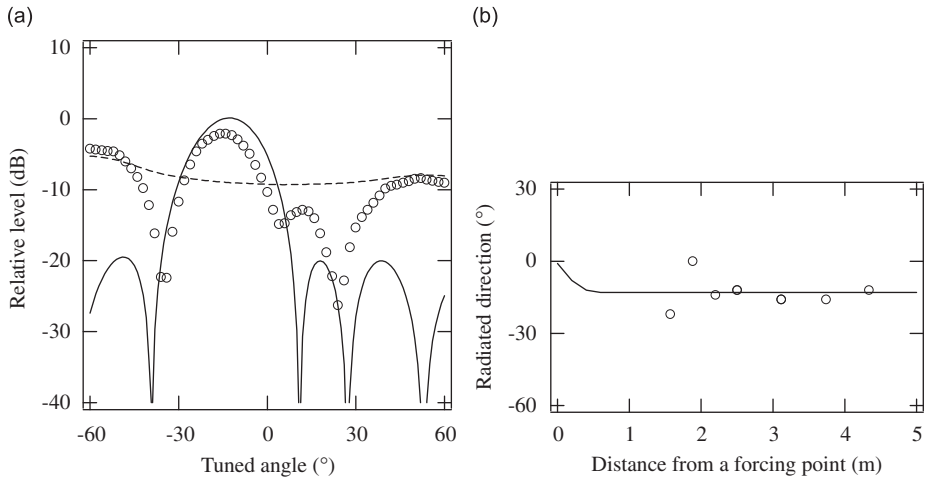

Fig. 12. Measured and predicted results for vertical shaker excitation at 1600 Hz. (a) Radiation pattern measured at a distance of 3.12 m from the forcing point. ○, Measured results; —, predictions for coherent sources; - - -, predictions for incoherent sources. (b) Direction of main lobe in the radiation pattern. ○, Measured results; —, predictions for coherent sources.

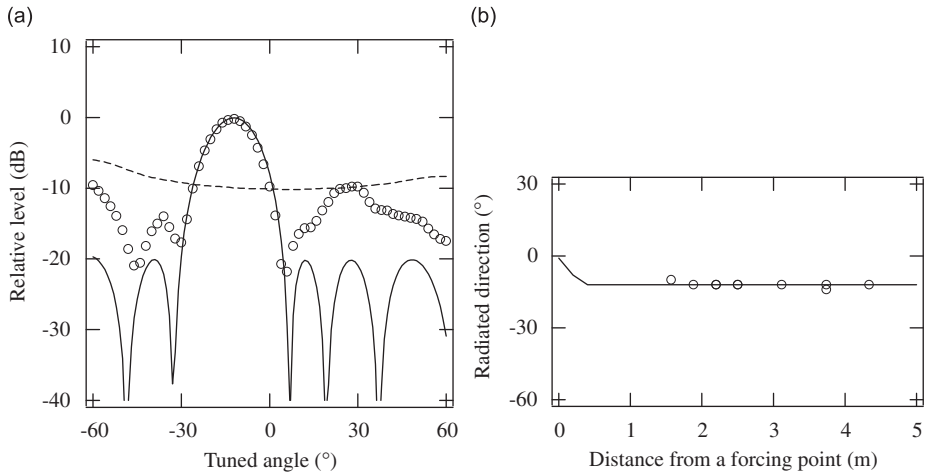

Fig. 13. Measured and predicted results for vertical shaker excitation at 2000 Hz. (a) Radiation pattern measured at a distance of 3.12 m from the forcing point. ○, Measured results; —, predictions for coherent sources; - - -, predictions for incoherent sources. (b) Direction of main lobe in the radiation pattern. ○, Measured results; —, predictions for coherent sources.

vibration). At frequencies associated with the pinned–pinned resonance, especially 1000 Hz for the vertical vibration, the predictions show less good agreement with the measurements. However, for 1600 Hz and above in the vertical direction and for most frequencies in the horizontal direction, agreement is excellent. This confirms the validity of the radiation model based on coherent sources and verifies the angle of principal radiation from the rail.

4. Measurements for a moving train

4.1. Description of the measurements

A measurement campaign has been carried out using moving trains and is used in a qualitative examination of the radiation properties of the rail. Quantitative analysis is more difficult due to the presence of other sources such as the wheels. In this section, an attempt is made to investigate the sound generated by the rail during a train pass-by by using a horizontal microphone array. The rails were 50N-type on concrete monobloc sleepers in ballast. The vertical rail pad stiffness was about 700 MN/m, which is stiffer than that used in the previous section but is of a similar type to that studied in [19]. The measurements were performed for vehicles with unpowered bogies, since these cars radiate mainly rolling noise, whereas the powered vehicles are known also to radiate traction motor fan noise [19].

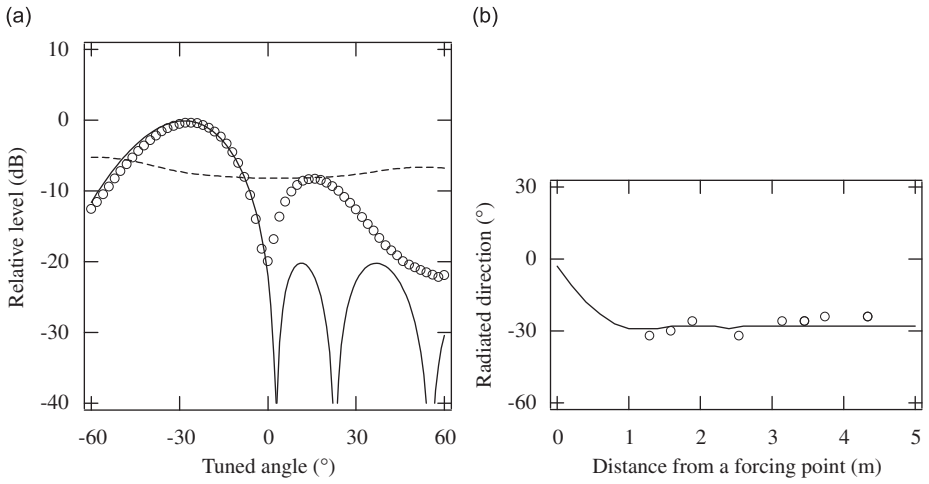

Fig. 14. Measured and predicted results for lateral shaker excitation at 630 Hz. (a) Radiation pattern measured at a distance of 3.12 m from the forcing point. ○, Measured results; —, predictions for coherent sources; - - -, predictions for incoherent sources. (b) Direction of main lobe in the radiation pattern. ○, Measured results; —, predictions for coherent sources.

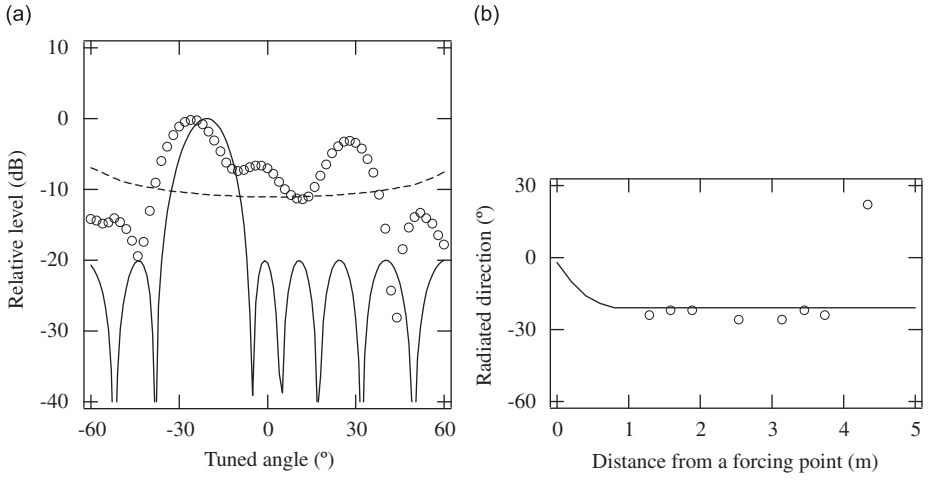

Fig. 15. Measured and predicted results for lateral shaker excitation at 1250 Hz. (a) Radiation pattern measured at a distance of 3.12 m from the forcing point. ○, Measured results; —, predictions for coherent sources; - - -, predictions for incoherent sources. (b) Direction of main lobe in the radiation pattern. ○, Measured results; —, predictions for coherent sources.

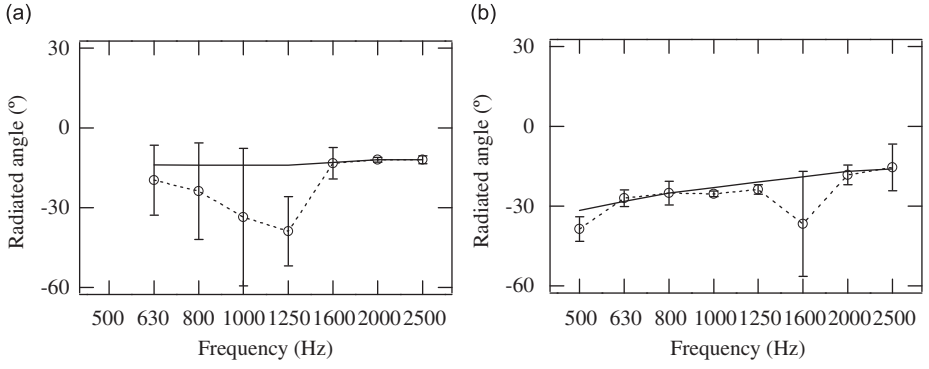

Fig. 16. Directivity of main lobe in the pattern of sound radiation from the rail. The microphone array is designed for a plane wave. Error bars are ± standard deviation. ○, Measured results; —, predictions for coherent sources. (a) Vertical shaker excitation, and (b) lateral shaker excitation.

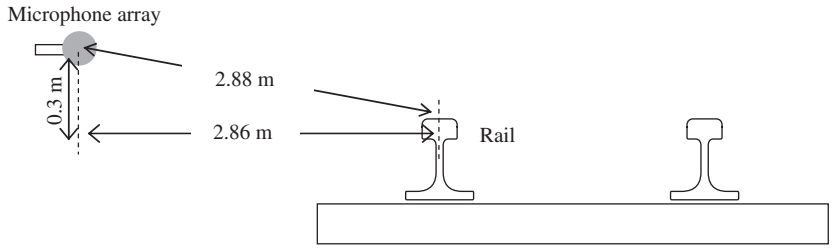

Fig. 17. Setup for the acoustic measurements from a running train.

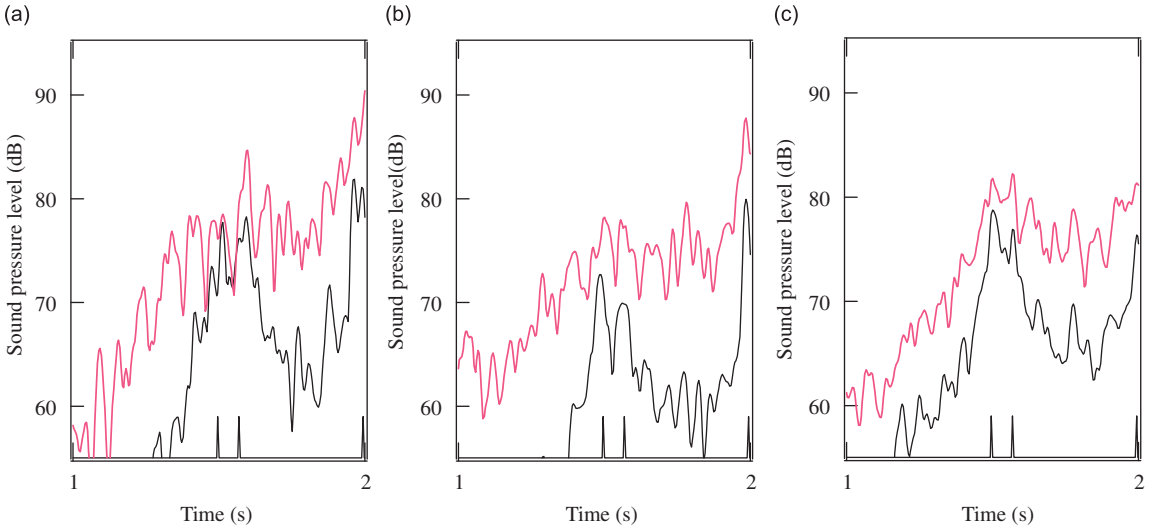

Fig. 18. Time histories filtered in one-third octave bands for a trailer bogie running at 102 km/h measured with the single microphone coloured line and microphone array. The array is designed for a plane wave with a tuned angle, ϕ=0°. —, Microphone array; —, single microphone. The positions of the wheels are indicated by the pulses at the bottom of the graph. (a) 500 Hz, (b) 1250 Hz, and (c) 2000 Hz.

The acoustic measurements were carried out with the same horizontal microphone array used in the shaker excitation experiments in Section 3. Fig. 17 shows the measurement setup. The microphone array was situated parallel to the rail at a distance of 2.88 m from the rail. In addition a single microphone was located at the centre of the array for comparison. A device to produce a pulse when a train wheel passes over it was mounted on one side of the railhead close to the position of the array.

4.2. Rail radiation for a moving train

The qualitative examination of the radiation behaviour of the rail is performed for different tuned angles, ϕ=−30° to +30°, of the microphone array. The array processing was based on an incoming plane wave, as in the previous section.

Fig. 18 shows the time histories of the sound pressure level measured with the single microphone and the microphone array directed at 0°. In each case results are filtered in one-third octave bands and results are shown for three such bands. The train was running at 102 km/h (28.3 m/s). Results are shown for a single unpowered bogie, which was the first bogie of the train. The positions of the wheels are indicated by the pulses at the bottom of the graph. It can be seen that the sources appear to be at the wheels, and that the sound levels measured with the array are considerably lower than the corresponding levels measured with the single microphone. This difference in level is primarily due to the different directivity of the single microphone and the array.

Figs. 19–21 show the time histories of the sound pressure level generated by the same bogie in these three frequency bands, obtained by steering the microphone array at various angles between −30° and +30°.

From Fig. 19, in the 500 Hz band, there is an apparent shift in the location of the maximum sound levels in the time histories. When the array axis is turned with a larger positive angle this shifts towards the left while for negative tuned angles it shifts towards the right. The rail is expected to be the dominant noise source at this frequency [5–7,19]. Moreover, in this frequency band, the decay rate of vertical vibration is high, but for lateral vibration it is lower. Thus it is expected that the lateral waves in the rail will be the dominant source of noise at this frequency.

There could be two possible reasons for the apparent lateral shift noted above. For a point source, changing the focus angle of the array would cause the source to be seen either before or after it passed in front of the microphones. However, it is found that this does not explain the observed results. For example, at a focus angle of 30° and a distance from the rail of 2.88 m, a point source would be detected at a location 1.66 m from the actual source position. For a speed of 28.3 m/s this would correspond to a time lag of 0.06 s, whereas the results in Fig. 19(c) indicate a larger shift of 0.13 s.

The second, and more plausible explanation for the apparent lateral shift in the time histories, is that it is associated with the large radiation from the propagating wave in the rail. This motion extends to each side of the wheel; the motion ahead of the wheel radiates sound that is detected by positive array angles, while that behind the wheel is detected by negative array angles. This asymmetry means that the peak in the array output is concentrated either before or after the wheel location and does not correspond to a source at the wheel position.

Moreover, it can be seen that, by directing the array at an angle of $\pm 30°$, the sound levels produced before or after the bogie passes in front of the array are greater than for 0°. Care is needed in interpreting differences in level as these may also occur due to the dependence of the width of the main lobe on the angle, and the fact that the source is further away as the

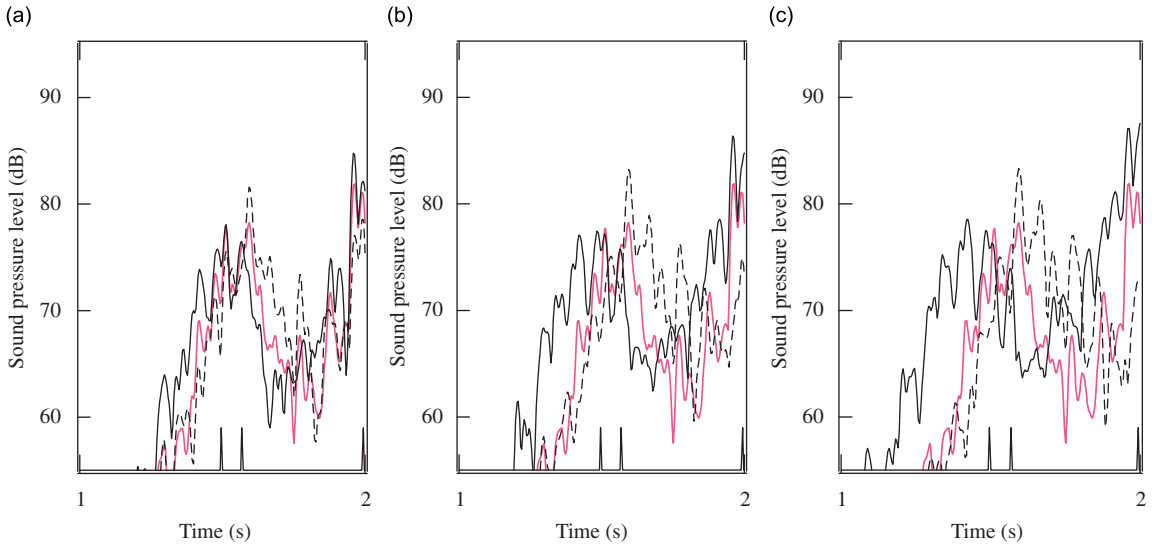

Fig. 19. Time histories of a trailer bogie running at 102 km/h measured with the microphone array, filtered in 500 Hz one-third octave band. The array is designed for a plane wave with a tuned angle, ϕ. The positions of the wheels are indicated by the pulses at the bottom of the graph. (a) —, ϕ=10°; - - -, ϕ=−10°; —, ϕ=0° coloured line. (b) —, ϕ=20°; - - -, ϕ=−20°; —, ϕ=0° coloured line. (c) —, ϕ=30°; - - -, ϕ=−30°; —, ϕ=0° coloured line.

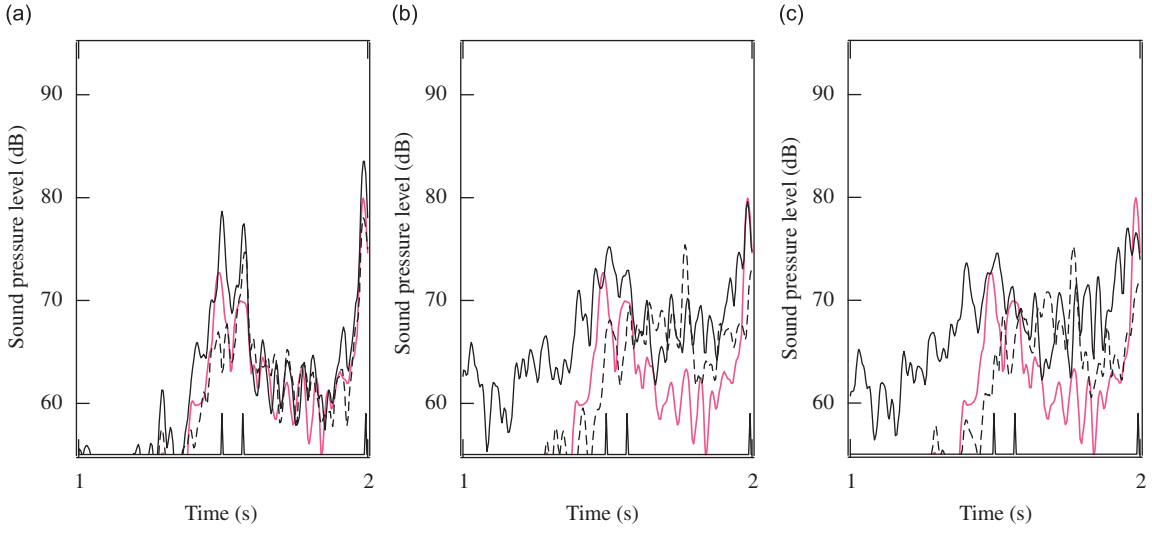

Fig. 20. Time histories of a trailer bogie running at 102 km/h measured with the microphone array, filtered in 1250 Hz one-third octave band. The array is designed for a plane wave with a tuned angle, ϕ. The positions of the wheels are indicated by the pulses at the bottom of the graph. (a) —, ϕ=10°; - - -, ϕ=−10°; —, ϕ=0° coloured line. (b) —, ϕ=20°; - - -, ϕ=−20°; —, ϕ=0° coloured line. (c) —, ϕ=30°; - - -, ϕ=−30°; —, ϕ=0° coloured line.

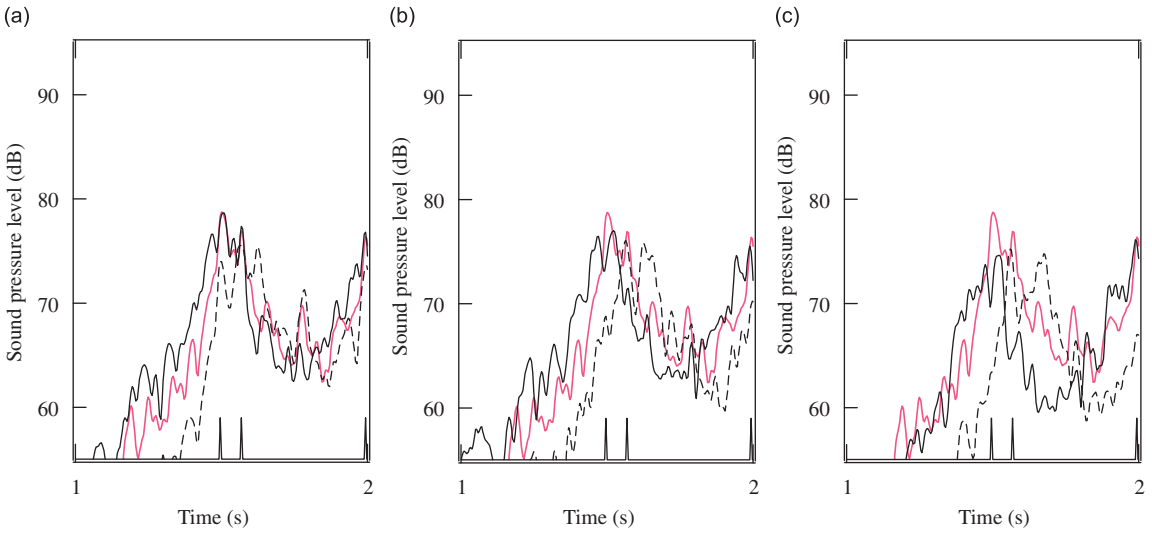

Fig. 21. Time histories of a trailer bogie running at 102 km/h measured with the microphone array, filtered in 2000 Hz one-third octave band. The array is designed for a plane wave with a tuned angle, ϕ. The positions of the wheels are indicated by the pulses at the bottom of the graph. (a) —, ϕ=10°; - - -, ϕ=−10°; —, ϕ=0° coloured line. (b) —, ϕ=20°; - - -, ϕ=−20°; —, ϕ=0° coloured line. (c) —, ϕ=30°; - - -, ϕ=−30°; —, ϕ=0° coloured line.

angle increases. Nevertheless, it may be noted that, at this angle, the array is focussed in a direction that is close to the supersonic structural radiation from the lateral rail vibration (the lateral rail vibration radiates at an angle of about 28° at this frequency, Fig. 16(b)) at which one would expect a strong output.

Fig. 20 shows corresponding results for 1250 Hz. By steering the array axis at positive angles, there is an apparent increase in the sound levels before the bogie runs in front of the array, although the peak in the time histories shifts only slightly to the left. Conversely, by directing the array at negative angles, the sound levels in the time history are increased after the bogie passes in front of the array. There is a larger peak in the sound levels obtained by steering the array at 10°, although this peak is reduced for larger tuned angles. These results are consistent with radiation from vertical bending waves in the rail, which radiate sound at an angle of 13° to the normal due to free wave propagation at this frequency (Fig. 16(a)).

For 2000 Hz, it can be seen from Fig. 21 that, by turning the focus of the array, the increase of the sound levels in the time histories occurs apparently before or after the bogie passes in front of the array. This indicates that the array detects the radiation behaviour of the rail even in this frequency range where the wheel has a significant contribution to the total noise. This is also due to the fact that free wave propagation occurs in the rail, and this leads to an under-estimation of the contribution of the rail component of noise if the microphone array is steered at 0°.

Therefore, although they are only qualitative, these results confirm that, when it is directed normal to the rail, a microphone array does not detect a large part of the noise radiated from the rail. On the other hand it has been shown that radiation from the rail can be detected by focussing the array at an appropriate angle. If a swept focus is used that covers a sufficiently broad range of angles it can be expected that the rail radiation will be detected, although care is required in the appropriate weighting of different angles of incidence if a calibrated source level is to be obtained. However, this is beyond the scope of the present investigation.

5. Conclusions

The acoustic radiation from a vibrating rail has been investigated using an equivalent source model. The structural wave motion forms an extended source of sound radiation. The distribution of sound intensity in the horizontal plane has been shown to consist of sound propagating at a specific angle to the normal, which depends on the ratio of the wavenumbers in the rail and in air. This cannot be described simply as a directivity as the sound source is not compact, the intensity vectors are not radial and the angular distribution is not independent of radial distance.

Measurements of rail radiation using a microphone array have shown that the model based on an array of coherent sources gives reliable results. The output from the microphone array has its maximum when the tuned angle corresponds to the angle of radiation and good agreement is found with the model.

Measurements have also been taken of a moving train using a microphone array with different focus angles. These results agree qualitatively with the analysis using the model, although the presence of other sources makes exact comparison difficult.

The results of this study confirm that a microphone array orientated normal to the track cannot detect the sound radiation from a propagating wave in the rail. As shown in [19], it may under-estimate the rail component of noise by at

least 10 dB in the frequency region where waves propagate in the rail. An interesting consequence would be that a rail damper which reduces rail noise by increasing the decay rate [30], would produce no significant difference when measured using a microphone array orientated in this way.

It has been shown that radiation from the rail can be detected by focussing the array at an appropriate angle. If a swept focus is used that covers a sufficiently broad range of angles it can be expected that the rail radiation will be detected, although it would be difficult to obtain a calibrated source level from such a method.

Appendix A

The motion of a Timoshenko beam is described by its deflection u and the rotation of the cross-section relative to the undeformed axis, ϕ. The equations of motion for a Timoshenko beam on an elastic foundation of stiffness s per unit length excited by a point force at x=0 can be written in the form [31]

$$GA\kappa\frac{\partial}{\partial x}\left(\phi-\frac{\partial u}{\partial x}\right)+su+\rho A\frac{\partial^2 u}{\partial t^2}=F\delta(x)e^{i\omega t} \tag{A1}$$

$$GA\kappa\left(\phi-\frac{\partial u}{\partial x}\right)-EI\frac{\partial^2\phi}{\partial x^2}+\rho I\frac{\partial^2\phi}{\partial t^2}=0 \tag{A2}$$

where ρ is the density of steel, E is Young's modulus, G is the shear modulus, A is the cross-sectional area, I is the second moment of area and $\kappa<1$ is the shear coefficient. The sleeper mass, etc. can be included in the support stiffness by making $s(\omega)$ frequency-dependent according to

$$s(\omega)=\frac{s_p(s_b-\omega^2 m_s')}{(s_p+s_b-\omega^2 m_s')} \tag{A3}$$

where s_p is the pad stiffness per unit length, s_b is the ballast stiffness per unit length and m'_s is the sleeper mass per unit length along the track. Hysteretic damping can be included by making these stiffnesses, as well as E and G, complex.

Considering harmonic motion at frequency ω, free wave solutions can exist of the form

$$u(xt)=Ue^{i\omega t}e^{-ikx} \tag{A4}$$

$$\phi(x,t)=U\Psi e^{i\omega t}e^{-ikx} \tag{A5}$$

where U is the complex amplitude and $U\Psi$ is the corresponding amplitude of ϕ. Substituting these into Eq. (A2) yields,

$$\Psi=\frac{-ikGA\kappa}{\rho I\omega^2-GA\kappa-EIk^2} \tag{A6}$$

which differs for the two waves (propagating and evanescent). Substituting this into Eq. (A1) gives a quadratic equation for k^2

$$k^4+C_2(\omega)k^2+C_3(\omega)=0 \tag{A7}$$

where, as in [25]

$$C_2(\omega)=\left(\frac{s-m_r'\omega^2}{GA\kappa}\right)-\left(\frac{\rho I\omega^2}{EI}\right) \tag{A8}$$

and

$$C_3(\omega)=\left(\frac{s-m_r'\omega^2}{EI}\right)\left(1-\frac{\rho I\omega^2}{GA\kappa}\right) \tag{A9}$$

Once free wave motion has cut on, Eq. (A7) has one positive and one negative solution for k^2 provided that $C_3>0$. The corresponding values of k are denoted $\pm k_1$, corresponding to the propagating waves, and $\pm k_2=\mp i\beta_2$ for the evanescent waves. Due to damping k_1 and β_2 have small imaginary parts.

The solution for the point mobility can be found by using a method similar to Grassie [25]. Taking Fourier transforms of Eq. (A1) from the spatial to the wavenumber domain gives

$$(GA\kappa ik(\Psi-ik)+s-m_r'\omega^2)U(k)=F \tag{A10}$$

which can be rearranged to give

$$\frac{U}{F}=\frac{1}{GA\kappa}\left(\frac{k^2+C_1(\omega)}{k^4+k^2C_2(\omega)+C_3(\omega)}\right) \tag{A11}$$

where C_2 and C_3 are given by Eqs. (A8) and (A9) and

$$C_1(\omega)=\frac{GA\kappa}{EI}-\frac{\rho I\omega^2}{EI} \tag{A12}$$

Finally, taking the inverse Fourier transform, the transfer mobility for a response position x is given by

$$Y(x) = \frac{\mathrm{i}\omega u(x)}{F} = \frac{\mathrm{i}\omega}{2\pi}\int_{-\infty}^{\infty} \frac{1}{GA\kappa}\left(\frac{k^2 + C_1(\omega)}{k^4 + k^2 C_2(\omega) + C_3(\omega)}\right)\mathrm{e}^{-\mathrm{i}kx}\,\mathrm{d}k \tag{A13}$$

This can be determined using an appropriate contour integration. For $x \geq 0$, the contour should be closed at infinity in the lower half plane. The poles of the integrand are the free wavenumbers, which are the solutions to Eq. (A7). The integral is equal to $-2\pi\mathrm{i}$ times the sum of the residues of the poles enclosed by the contour,

$$Y(x) = \frac{-\mathrm{i}\omega}{2\pi} 2\pi\mathrm{i} \sum_{n \text{ with } \mathrm{Im}(k_n)<0} \mathrm{Res}(k_n) \text{for } x \geq 0 \tag{A14}$$

the residues being given by

$$\mathrm{Res}(k_n) = \frac{\mathrm{e}^{-\mathrm{i}k_n x}}{GA\kappa}\left(\frac{k_n^2 + C_1(\omega)}{4k_n^3 + 2k_n C_2(\omega)}\right) \tag{A15}$$

where the poles are the free wavenumber solutions, k_1 and k_2. Hence the mobility can be written as

$$Y(x) = (u_1 \mathrm{e}^{-\mathrm{i}k_1|x|} - \mathrm{i}u_2 \mathrm{e}^{-\beta_2|x|}) \tag{A16}$$

where

$$u_1 = \frac{\omega}{GA\kappa}\left(\frac{k_1^2 + C_1(\omega)}{4k_1^3 + 2k_1 C_2(\omega)}\right) \tag{A17}$$

and

$$u_2 = \frac{\omega}{GA\kappa}\left(\frac{-\beta_2^2 + C_1(\omega)}{4\beta_2^3 - 2\beta_2 C_2(\omega)}\right) \tag{A18}$$

References

[1] D.J. Thompson, C.J.C. Jones, A review of the modelling of wheel/rail noise generation, *Journal of Sound and Vibration* 231 (3) (2000) 519–536.
[2] C. Talotte, Aerodynamic noise, a critical survey, *Journal of Sound and Vibration* 231 (2000) 549–562.
[3] P.E. Gautier, F. Poisson, F. Létourneaux, High speed train external noise: recent results in the TGV case, *19th International Congress on Acoustics*, Madrid, September 2007.
[4] C. Mellet, F. Létourneaux, F. Poisson, C. Talotte, High speed train noise emission: latest investigation of the aerodynamic/rolling noise contribution, *Journal of Sound and Vibration* 293 (2006) 535–546.
[5] D.J. Thompson, B. Hemsworth, N. Vincent, Experimental validation of the TWINS prediction program, part 1: method, *Journal of Sound and Vibration* 193 (1996) 123–135.
[6] D.J. Thompson, P. Fodiman, H. Mahé, Experimental validation of the TWINS prediction program, part 2: results, *Journal of Sound and Vibration* 193 (1996) 137–147.
[7] C.J.C. Jones, D.J. Thompson, Extended validation of a theoretical model for railway rolling noise using novel wheel and track designs, *Journal of Sound and Vibration* 267 (2003) 509–522.
[8] D.J. Thompson, Predictions of acoustic radiation from vibrating wheels and rails, *Journal of Sound and Vibration* 120 (1988) 275–380.
[9] J.D. van der Toorn, H. Hendricks, T.C. van den Dool, Measuring TGV source strength with syntacan, *Journal of Sound and Vibration* 193 (1996) 113–121.
[10] B. Barsikow, Experiences with various configurations of microphone arrays used to locate sound sources on railway trains operated by the DB AG, *Journal of Sound and Vibration* 193 (1996) 283–293.
[11] S. Brühl, A. Röder, Acoustic noise source modelling based on microphone array measurements, *Journal of Sound and Vibration* 231 (2000) 611–617.
[12] C. Hanson, B. Barsikow, Noise sources on Amtrak's high speed train, *Proceedings of Inter Noise 2000*, Nice (France), August 2000.
[13] B. Barsikow, W.F. King III, E. Pfizenmaier, Wheel/rail noise generated by a high-speed train investigated by a line array of microphones, *Journal of Sound and Vibration* 118 (1987) 99–122.
[14] M.G. Dittrich, M.H.A. Janssens, Improved measurement methods for railway rolling noise, *Journal of Sound and Vibration* 231 (2000) 595–609.
[15] G. Hölzl, Low noise goods wagons, *Journal of Sound and Vibration* 193 (1996) 359–366.
[16] A. Nordborg, A. Martens, J. Wedemann, L. Willenbrink, Wheel/rail noise separation with microphone array, *Proceedings of Inter Noise 2001*, The Hague (Netherlands), August 2001.
[17] K.G. Degen, A. Nordborg, A. Martens, J. Wedemann, L. Willenbrink, M. Bianchi, Spiral array measurements of high-speed train noise, *Proceedings of Inter Noise 2001*, The Hague (Netherlands), August 2001.
[18] T. Kitagawa, Y. Zenda, Y. Abe, Y. Ogata. Sound radiated by vibration of railway wheels, *Proceedings of Inter Noise 2001*, The Hague (Netherlands), August 2001.
[19] T. Kitagawa, D.J. Thompson, Comparison of wheel/rail noise radiation on Japanese railways using the TWINS model and microphone array measurements, *Journal of Sound and Vibration* 293 (2006) 496–509.
[20] D.J. Thompson, C.J.C. Jones, Sound radiation from a vibrating railway wheel, *Journal of Sound and Vibration* 253 (2002) 401–419.
[21] K. Knothe, S.L. Grassie, Modelling of railway track and vehicle/track interaction at high frequencies, *Vehicle System Dynamics* 22 (1993) 209–262.
[22] D.J. Thompson, Experimental analysis of wave propagation in railway tracks, *Journal of Sound and Vibration* 203 (1997) 867–888.
[23] D.J. Thompson, N. Vincent, Track dynamic behaviour at high frequencies. Part 1: theoretical models and laboratory measurements, *Vehicle System Dynamics Supplement* 24 (1995) 86–99.
[24] N. Vincent, D.J. Thompson, Track dynamic behaviour at high frequencies. Part 2: experimental results and comparisons with theory, *Vehicle System Dynamics Supplement* 24 (1995) 100–114.
[25] S.L. Grassie, R.W. Gregory, D. Harrison, K.L. Johnson, The dynamic response of railway track to high frequency vertical excitation, *Journal of Mechanical Engineering Science* 24 (1982) 77–90.
[26] C.J.C. Jones, D.J. Thompson, R.J. Diehl, The use of decay rates to analyse the performance of railway track in rolling noise generation, *Journal of Sound and Vibration* 293 (2006) 485–495.

[27] D.J. Thompson, C.J.C. Jones, N. Turner, Investigation into the validity of two-dimensional models for sound radiation from waves in rails, *Journal of the Acoustical Society of America* 113 (2003) 1965–1974.
[28] M.A. Heckl, Railway noise—can random sleeper spacings help?, *Acoustica* 81 (1995) 559–564.
[29] T. Kitagawa, *An Investigation into Inconsistencies between Theoretical predIctions and Microphone Array Measurements of Railway Rolling Noise*, Ph.D. Thesis, University of Southampton, 2007.
[30] D.J. Thompson, C.J.C. Jones, T.P. Waters, D. Farrington, A tuned damping device for reducing noise from railway track, *Applied Acoustics* 68 (2007) 43–57.
[31] K.F. Graff, *Wave Motion in Elastic Solids*, Dover Publications, New York, 1991.